Sensor and Simulation Notes

Note 382

4 July 1995

A Reflector Antenna for Radiating Impulse-Like Waveforms

D. V. Giri and H. Lackner

Pro-Tech, 3708 Mt. Diablo Blvd, Suite 215 Lafayette, CA 94549

I. D. Smith and D. W. Morton

Pulse Sciences, Inc., 600 McCormick Street, San Leandro, CA 94577

and

C. E. Baum, J. R. Marek, D. Scholfield, and W. D. Prather

Phillips Laboratory, Kirtland AFB, NM 87117

Abstract

A paraboloidal reflector antenna fed by a pyramidal horn has found widespread application in radar and communication engineering. However, the reflector antenna has very useful characteristics when it is fed or illuminated by two or four-conductor transmission lines. We have analyzed, designed, fabricated, and tested a reflector antenna fed by a pair of conical transmission lines connected in parallel at the focal point. The voltage waveform at the apex of the lines, is a fast rising ($\sim$ 100 ps), slowly decaying ($\sim$ 20 ns e-fold) pulse with a peak amplitude of about 125 kV. The calculated and measured radiated field at a distance of 304 m is impulse-like with amplitude of about 4.2 kV/m and a pulse duration of $<$ 200 ps. The resultant wide spectrum of the radiated field, extending from about 50 MHz to few GHz, is expected to find many applications in areas such as hostile target identification, buried object detection, high-power jamming etc.

1. Introduction

A finite sized antenna that can radiate a true impulse into the far field is impossible, from physical considerations. However, a dispersionless and wideband antenna with a nearly flat radiated spectrum is desirable for many applications, such as hostile target identification, buried object detection, electronic warfare etc. It is the purpose here to describe the working principles, design considerations, fabricational details and performance data of an impulse radiating antenna (IRA) system. This type of an IRA employs a paraboloidal reflector fed by transverse electromagnetic (TEM) lines. Such a radiating system has been termed "the reflector IRA" for ease of reference. It is an example of aperture type of antennas. It is well known that the radiated field from an aperture antenna consists of a spatial integration of the aperture fields over the aperture, while the temporal behavior of the aperture field gets differentiated in the far field. For example, if the aperture is illuminated by a step-function electric field of constant amplitude, then the radiated field would be an impulse function. Since, ideal step functions and ideal impulse functions are impractical, the physical antenna radiates an impulse-like function with an extremely high bandwidth, satisfying the physical constraint that there be no dc component in the radiated spectrum. No radiated dc component also means that the total area under the time domain radiated electric or magnetic field must vanish.

Since we are dealing with impulse-like radiated fields, the spectral content can range from 10's of MHz to several GHz. The low frequency (f_ℓ) radiation is limited by the antenna size, while the high frequency (f_h) limitation is imposed by the non-zero risetime of the voltage pulse fed to the TEM lines that illuminate the paraboloidal reflector. Since the feed is TEM, the antenna is dispersionless, unlike other "frequency-independent antennas" such as log-periodic antennas. Some of the bandwidth definitions in the present context are

$$\text{bandwidth} = f_h - f_\ell$$

$$\text{percentage bandwidth} = \frac{f_h - f_\ell}{[(f_h + f_\ell)/2]} \times 100$$

$$= \begin{cases} < 1\% & \text{narrowband (e.g., AM radio)} \\ 1 \text{ to } 25\% & \text{wideband (e.g., TV signals)} \\ > 25\% & \text{ultrawideband (e.g., none in the IEEE dictionary)} \end{cases}$$

The reflector IRA described here has a percentage bandwidth in excess of 180% out of a

maximum of 200%, suggesting the need to at least add another category in the percentage bandwidth definition. One could define a bandratio ($= f_h/f_\ell$) instead of the bandwidth, in which case, the bandratio for the prototype IRA is about 60.

Since it was first proposed in 1989 [1], many aspects of the reflector IRA have been analyzed in the past. These include feed configurations [2], aperture efficiencies [3], antenna analysis [4 to 6], low-frequency performance [7] and feed impedance [8]. Additional analytical expressions, quantifying the diffractions from the launcher plates and the circular rim of the reflector were developed in [9], and certain fabricational details described in [10 to 13]. Based on the analytical and design considerations described in [1 to 13], a prototype IRA using a 3.66 m diameter reflector fed by a pair of 400 Ω TEM conical transmission lines connected in parallel, has been built and tested. We describe the expected and measured performance as well as some optimization (e.g., use of electromagnetic lens in the feed) techniques, in the following sections.

2. Working Principles of a Reflector IRA

The reflector IRA under consideration consists of a paraboloidal reflector fed by two pairs of coplanar feed plates as illustrated in figure 1. Coplanar feed plates are chosen over the more conventional facing-plate geometry to minimize the aperture blockage effects. Again, to reduce the aperture blockage, the feed plates are required to be narrow, resulting in high-values (several 100′ of Ω) of feed impedance. Two 400 Ω lines are connected in parallel resulting in a net feed impedance of 200 Ω. The aperture area should be as large as practical, since the far field is proportional to the square root of this area for a constant voltage at the feed. The far field is proportional to the aperture area for a constant aperture field. The pulse generator has to be of the differential type to avoid common mode currents on the feed plates, which could distort the desired features in the far field. The pulse generator can be represented by a single switch near the focal point. The two electrodes of the switch have a potential difference of $V(t) = \pm(V_0/2)u(t)$. Since the far field on axis is proportional to $(\partial V/\partial t)$, it is desirable to maximize this rate of rise. We have achieved a rate of rise of $> 10^{15}$ V/s. The combination of requiring physically small switches, high voltages and fast rise times implies the use of electromagnetic lenses in the switch region. The lens can be made of an oil medium which serves the dual purposes of high-voltage insulation and ensuring a spherical TEM wave launch on to the feed plates.

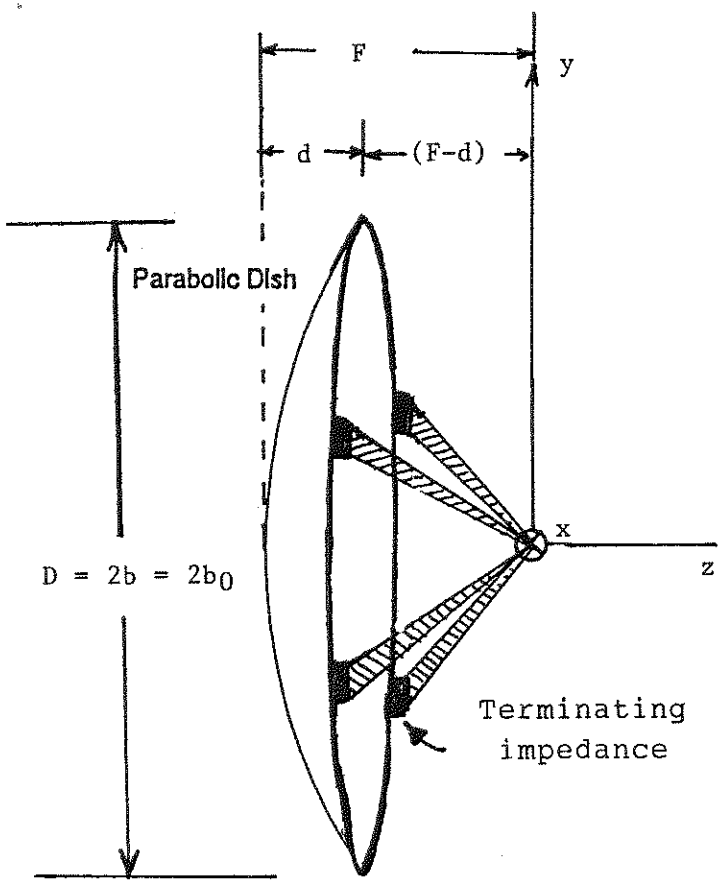

a) Side view x = 0 plane

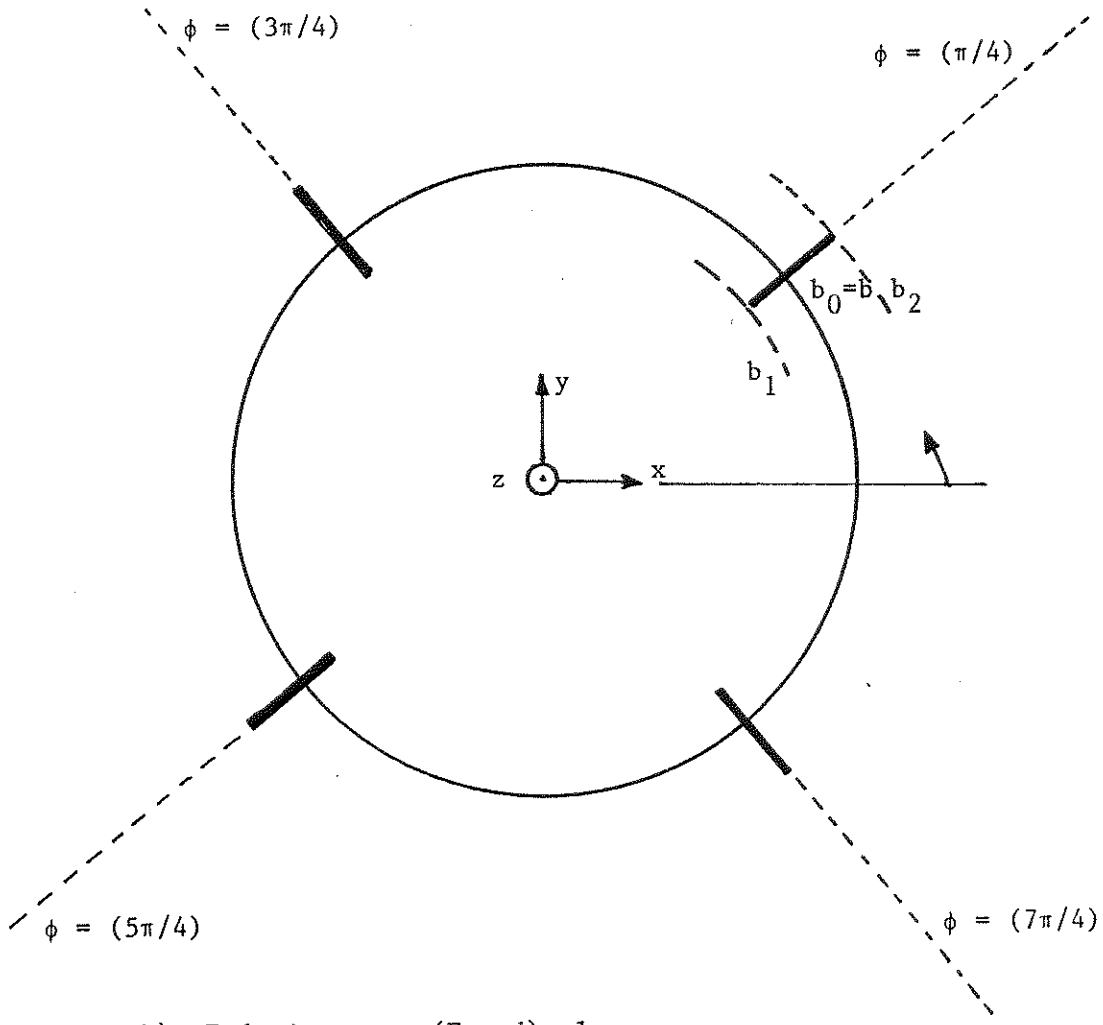

b) End view z = -(F - d) plane

Figure 1. An Illustration of a reflector fed by a pair of coplanar conical TEM lines

The detailed design considerations are described in later section.

Next, we look at an estimation of boresight waveforms. For analysis purposes, one could consider a 2 coplanar plate feed (figure 2), although in practice we used 2 such feed lines connected in parallel for a more uniform illumination of the reflector. When the reflector IRA was originally proposed [1], the boresight radiation was predicted to consist of a feed-step followed by an impulse-like behavior as indicated in figure 3. A more recent analysis [9] has extended the results of figure 3, by chronologically considering the various temporal elements of the boresight radiation. Let us assume that the voltage pulse generator is switched on at $t = 0$, and the observer is at a distance r $(= z)$ to the right of the focal point of the paraboloid. These elements are:

A. *Prepulse*

1) feed step

B. *Main pulse of interest*

2) impulse

C. *Postpulse*

3) feed plate diffraction consisting of two parts

a) plate edge on plate of finite width, large compared to wavelength

b) plate of finite width, small compared to wavelength, modelled by circular cylinder

4) edge diffraction from the circular rim of the paraboloidal reflector

D. *Constraints on entire pulse*

5) low-frequency dipole moment radiation and no radiation at zero frequency (dc).

All of the above, have been analyzed in the past, but summarized here for completeness.

Prepulse or feed step

This is a direct radiation from source or the "switch" towards the observer. It has a negative amplitude for the assumed signs of voltages on launcher plates. For the geometry in figure 2, under the assumption of narrow plates (plate width << plate separation), the feed step is given by [5],

$$E_{y1}(r,\, t) = -\frac{V_0}{r}\,\frac{D}{4\pi f_g}\,\frac{1}{2F}\left[u(t - t_r) - u\left(t - \left(t_v + \frac{2F}{c}\right)\right)\right] \tag{1}$$

where

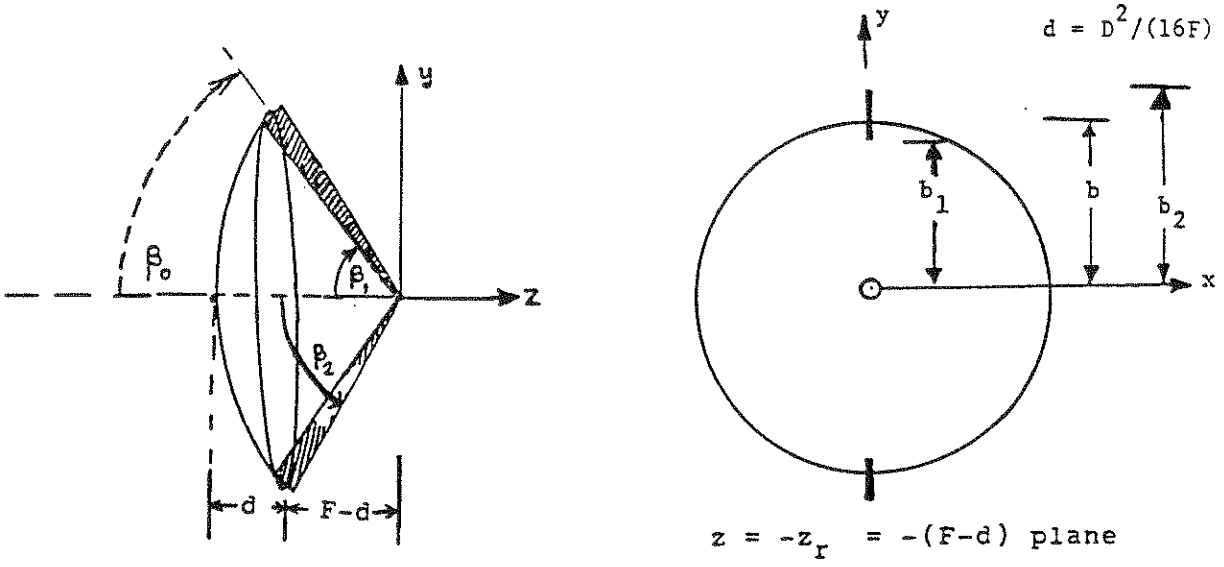

Figure 2. The reflector IRA fed by one coplanar-plate conical line

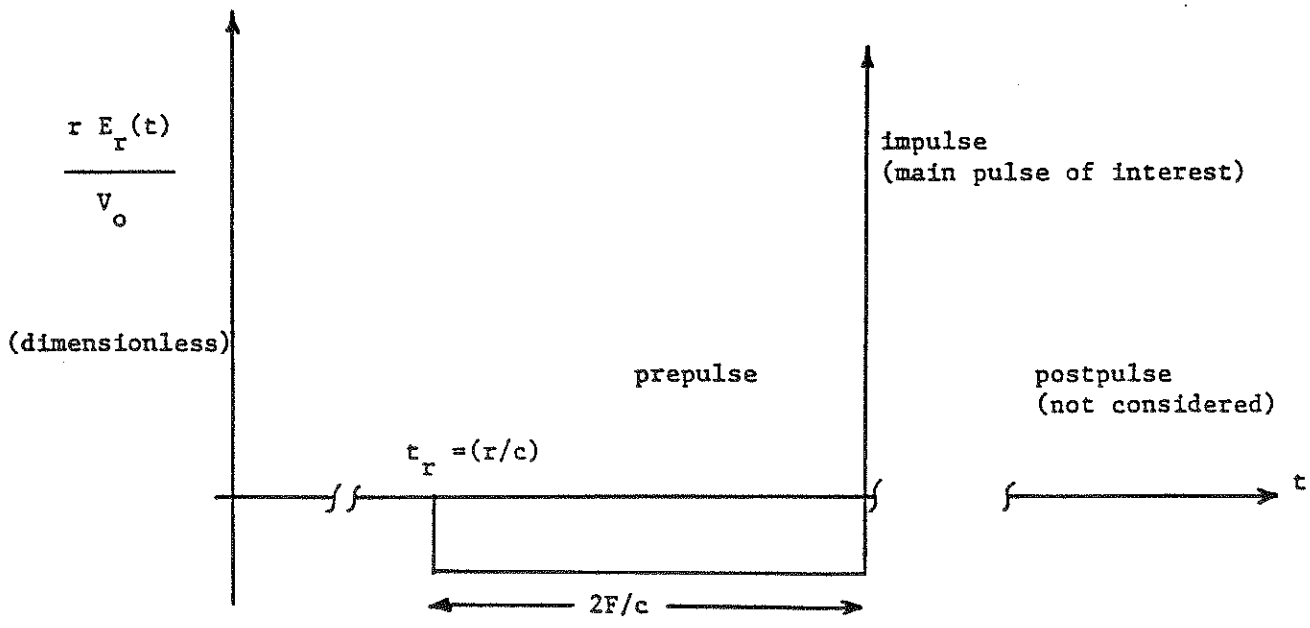

Figure 3. Far field on axis from a reflector IRA fed by an ideal step function [1]

V_0 = potential difference between the feed plates, D = diameter of the reflector F = focal length of the reflector, $t_r = r/c$ = time of arrival at the observer, f_g = geometrical impedance factor = Z_c/Z_0, with Z_c = TEM characteristic impedance of the feed line and Z_0 is the characteristic impedance of free space.

Impulse at $t = [t_r + (2F/c)]$

The impulse-like radiation occurs at a time $t = [t_r + (2F/c)]$ for an observer location on axis. The impulse amplitude is given by [5],

$$E_{y2}(r,\, t) = \frac{V_0}{r}\, \frac{h_{a_y}}{2\pi c f_g}\, \delta\left(t - \left(t_r + \frac{2F}{c}\right)\right) \tag{2}$$

where the effective height is given by [8],

$$h_{a_y} = \frac{\pi m^{-1/4}}{K(m)}\, b\left[1 - \frac{2}{\pi} \arcsin\left(\frac{1-\sqrt{m}}{1+\sqrt{m}}\right)\right] \tag{3}$$

and the parameter m is obtained by solving

$$f_g = \frac{Z_c}{Z_0} = \frac{K(m)}{K'(m)} \tag{4}$$

However, for narrow plates ($b_2 \rightarrow b_1$), the effective antenna height is $D/2$ and the impulse amplitude is

$$E_{y2}(r,\, t) \simeq \frac{V_0}{r}\, \frac{D}{4\pi c f_g}\, \delta\left(t - \left(t_r + \frac{2F}{c}\right)\right) \tag{5}$$

Feed – plate diffraction

The diffraction from the feed plates may be classified into two parts. As the spherical TEM wave launched by the feed plates scatters off the paraboloidal surface, it encounters the plate edges and then the plates themselves. These two parts have been derived in [9] and reproduced below:

$$E_{y_{3a}}(r,\, t) = -\frac{V_0}{r}\, \frac{1}{\sqrt{\sin(\beta_1)}} \left(\frac{1}{\sqrt{2}\,\pi^2}\right)\left(\frac{2}{3}\right) \sqrt{\frac{2a}{ct - (r+2F)}}\, u\left(t - \frac{r}{c} - \frac{2F}{c}\right) \tag{6a}$$

$$E_{y_{3b}}(r,\, t) \simeq -\frac{V_0}{r}\, \frac{1}{4\, \sin(\beta_0)}\, \frac{1}{\ell n\left[\frac{1}{\Gamma_e}\left\{\frac{2(ct-r)}{a_e\, \sin(\beta_0)} + 1\right\}\right]} + \cdots \tag{6b}$$

The plate edge diffraction signal of equation (6a) has been modelled by the classical diffraction from half-plane [14], while the diffraction from the plates of finite width ($\ll$ wavelength) is obtained by modelling the plates by equivalent round conductors of effective radius a_e. The parameter Γ_e in equation (6b) is the Euler's constant. It should be remarked that we have estimated the diffraction from the plates in 2 time regimes ($t < a/c$) and $(a/c) < t < (b/c)$ and obtained leading terms in an asymptotic sense. It is not clear how the two time regime solutions connect up. The diffraction from the launcher plates is of the opposite sign compared to the impulse-like radiation, initially falling off like $(1/\sqrt{t})$ (equation 6a) and behaves asymptotically like $(1/\ell n\sqrt{t})$ as seen in equation 6b.

Diffraction from the reflector edge

The diffracted signal from the circular rim of the reflector arriving at the observation point on axis has been estimated [9] in closed form. It is made easy by the fact that the illuminating TEM fields are parallel to the circular edge of the reflector. The result derived in [9] is

$$E_{y4}(r,\, t) = \frac{V_0}{4\pi r}\left(\frac{\pi}{2}\right)\frac{1-\sin(\beta_0/2)}{\cos(\beta_0/2)}\,\frac{1}{m^{1/4}K(m)} \left[1-\frac{2}{\pi}\arcsin\left(\frac{1-\sqrt{m}}{1+\sqrt{m}}\right)\right] u\left(t-\frac{r}{c}-\frac{2F}{c}\right) \tag{7}$$

This is the leading term in the rim-diffracted field on axis at a distance r on the optical axis. It is interesting to note that this field is of the same sign as the impulse-like waveform and of opposite sign to that of the launcher plate diffraction.

Finally, the radiation at low-frequencies may be characterized by a set of electric and magnetic dipole moments

$$\begin{aligned} \vec{p}(t) &= \vec{1}_y\; p_y \\ \vec{m}(t) &= -\vec{1}_x\; m_x \end{aligned} \tag{8}$$

with the resultant radiation along the $(\vec{p}\times\vec{m})$ direction which is the $+z$ axis, coinciding with the radiation at higher frequencies which is also along the $+z$ axis. Under a balance condition of $|\vec{m}| = c|\vec{p}|$, the low-frequency radiation pattern is a cardiod with a maximum along the boresight axis and null in the backward direction. So, the radiation from the reflector IRA along boresight direction, can be expressed as

$$\vec{E}_f(\vec{r}, t) = \vec{1}_y \; E_y(r, t)$$

$$E_y(r, t) = E_{y1}(r, t) + E_{y2}(r, t) + E_{y3}(r, t) + E_{y4}(r, t)$$
$$+ \text{ low-frequency radiation from dipole}$$
$$\text{moments resulting in time integral}$$
$$\text{constraints on entire pulse} \qquad (9)$$

This result of equation (9) is illustrated in figure 4. The time integral constraints imposed by the low-frequency radiation are (i) the complete first-time integral of the radiated waveform must be zero and (ii) the second-time integral must be proportional to the late-time dipole moments. With this analysis background, we now proceed to describe the design and performance data.

3. Design Considerations of the Prototype Reflector IRA

The prototype reflector IRA that has been fabricated and tested is shown in figure 5. It consists of a solid-surface, spun-aluminum, paraboloidal reflector of diameter $D =$ 3.66 m, focal length $F = 1.21$ m and $f_d = F/D = 0.33$. There are two pairs of coplanar conical lines, each with a TEM characteristic impedance of 400 Ω and the corresponding $f_g = 1.06$. The net impedance of the two lines is 200 Ω. The other geometrical parameters of the system, with reference to figure 1 are: $b = 1.830$ m, $b_1 = 1.585$ m, $b_2 = 2.105$ m, $d =$ depth of the reflector $= 0.69$ m, $\beta_0 = 74.29°$, $\beta_1 = 66.58°$, $\beta_2 = 82.30°$, and parameter $m = 0.5645$.

While the net feed impedance at the feed was designed to be 200 Ω by selecting the proper plate width to separation ratio, the actual fabrication of the terminating impedances (nominally 200 Ω at all four junctions between the plates and the reflector rim) needs to be experimentally optimized. The dc resistance of the termination of each of the two conical lines equals the TEM characteristic impedance, but the reactive part of the terminating impedances depends on how the series-parallel combination of resistors are assembled. A time-domain reflectometry (TDR) measurement using a TEK-109 (50 V, 180 ps rise pulse) was performed and the results are shown in figure 6. The initial geometry of the terminator consisted of a high capacitance and lowered voltage stand-off capability.

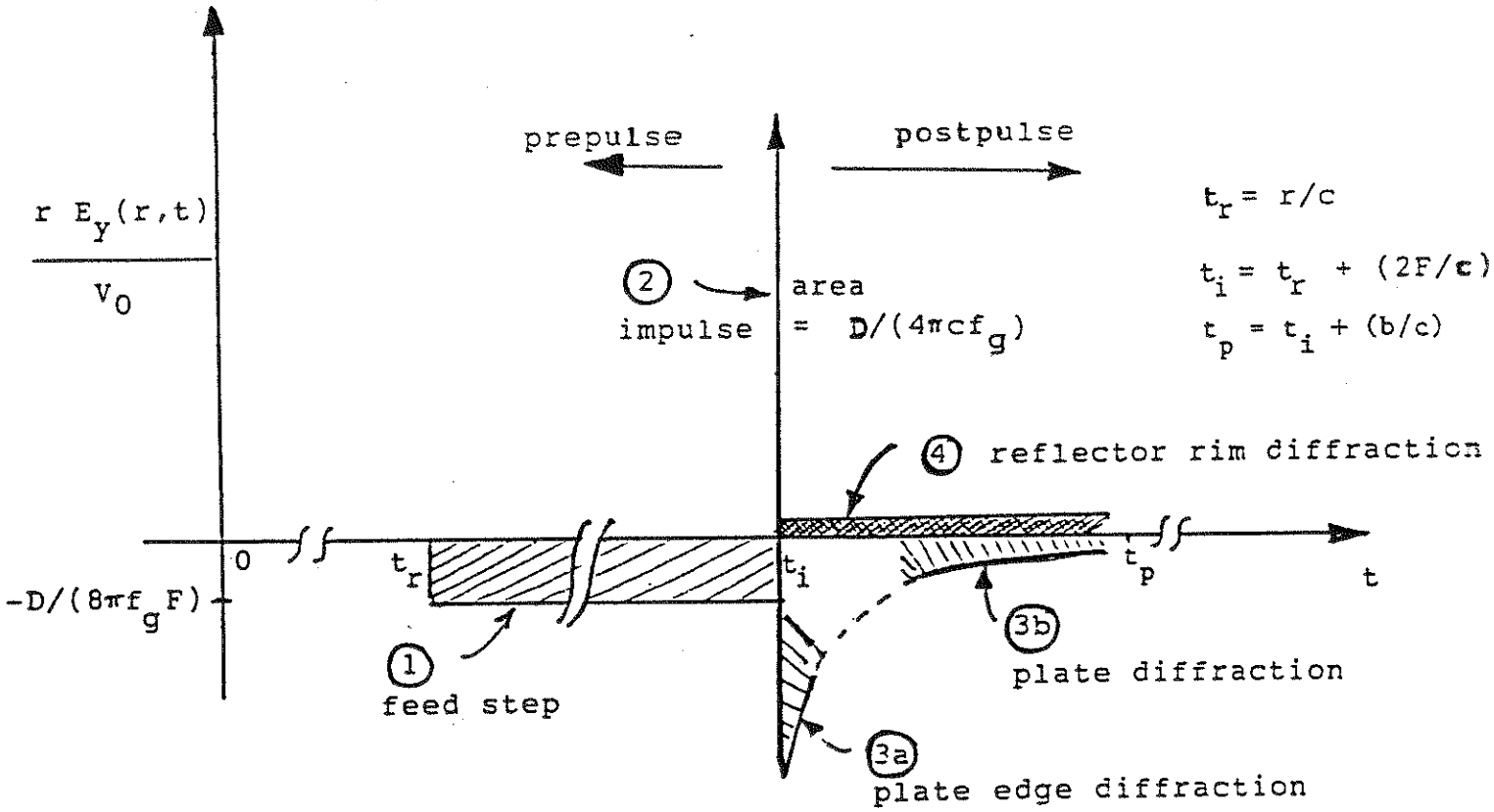

Figure 4. On axis radiation from a canonical reflector IRA of figure 2

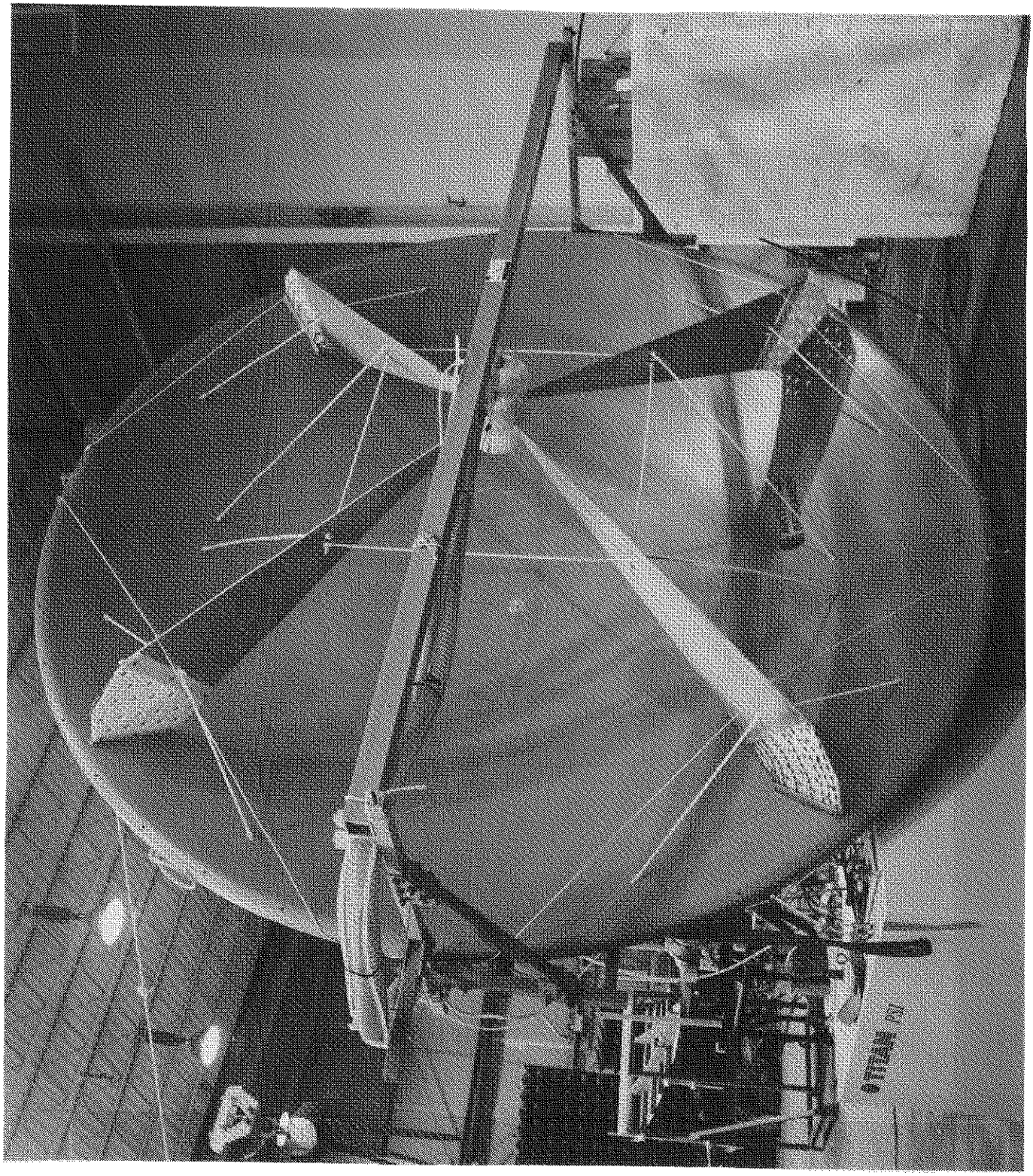

Figure 5. Photograph of the prototype reflector IRA

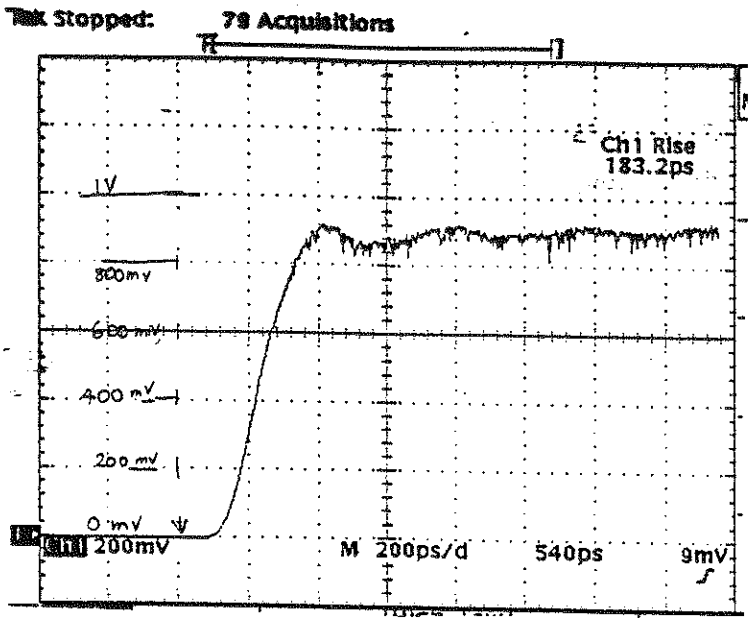

a) Input pulse for the TDR measurement (2V charge; ~185 ps rise)

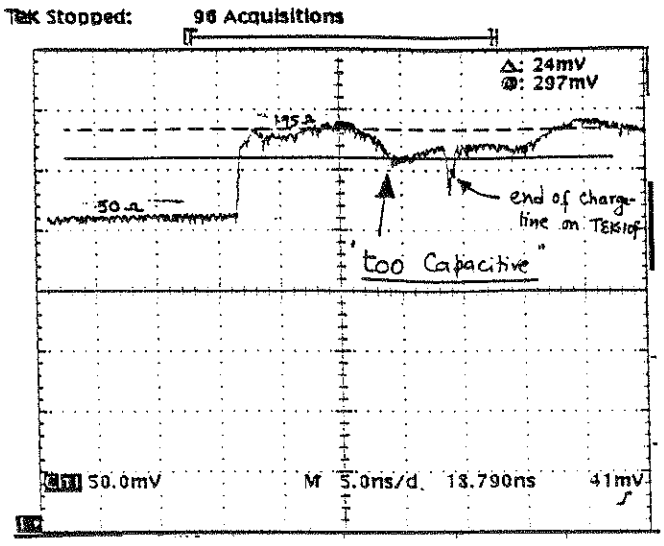

b) TDR data before "trimming"

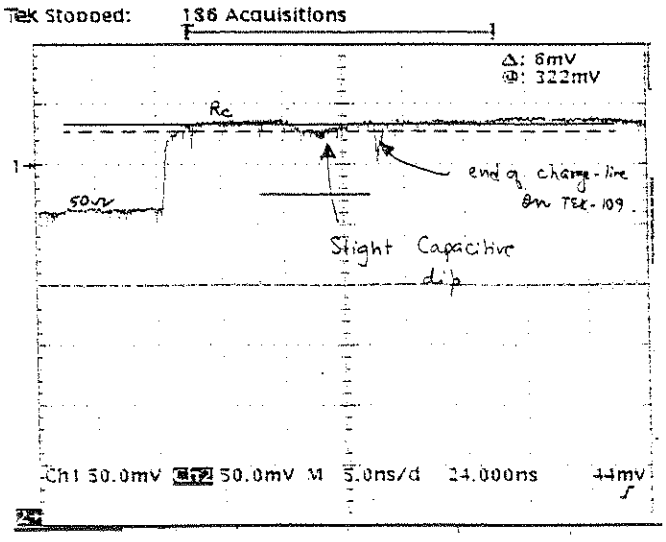

c) TDR data of the optimal terminator

Figure 6. TDR measurement for optimizing the terminating impedances

Through a sequence of "trimming" the geometry, we arrived at an optimal termination geometry. The average power in the pulse train, when the pulse generator is operated at 200 pulses per second, is of the order of 200 watts. This determined the number of 0.5 watt series resistors in each of the parallel chains of resistors. At a pulse repetition frequency (prf) of 200 Hz, the termination design worked well, but if the prf is upgraded to 1 kHz, the termination has to be suitably modified.

Next, we turn our attention to the launch region. A uniform dielectric, electromagnetic lens is included in the launch region to ensure the launching of an approximate spherical TEM wave onto the conical transmission lines. Inside the lens, we have an exact spherical TEM wave centered on the switch center. Outside the lens, it is an approximate spherical TEM wave centered at the focal point of the paraboloidal reflector. The (10–90)% risetime of the voltage pulse is of the order of 100 ps, which corresponds to a travel time of 3 cm in air and roughly 2 cm in the oil insulating medium surrounding the "switch" which represents the source. The switch consists of two conductors in a capsule that has high-pressure ($\sim$ 100 atm) hydrogen gas. The switch capsule is surrounded by oil as an insulator, in a dielectric container. The dielectric constant of the container material is chosen to be same as that of the oil medium. The oil medium, now serves two purposes of voltage standoff and an electromagnetic lens, which is achieved by shaping the oil container box. The cylindrical coordinate system (Ψ, z) at the feed is shown in figure 7 and the lens design consists of selecting h = cylindrical radius of the outermost ray and $\theta_{1_{\max}}$ = the angle made by the line inside the lens with respect to the direction of launch. Having selected these two parameters, we need to find the contour (Ψ/h, z/h) that ensures a spherical wavefront outside the oil box. The required equations are reproduced below from [15], in a step-by-step fashion suitable for computations

a) input $\quad h = 1,\ \mathcal{E}_r = 2.26,\ \theta_{2\max} = 74.29°,\ \theta_{1\max} = 90°$

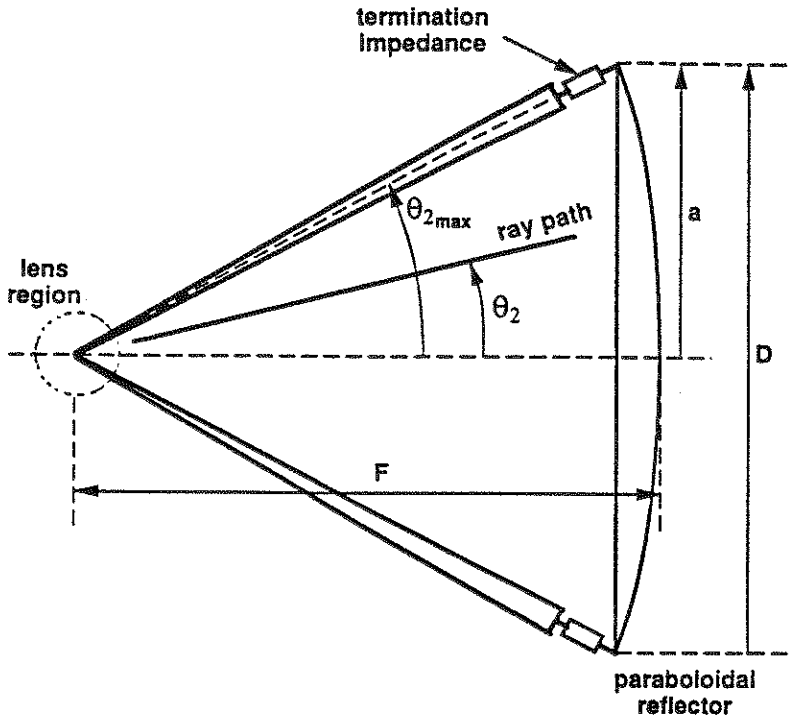

a) Schematic diagram of the prototype IRA

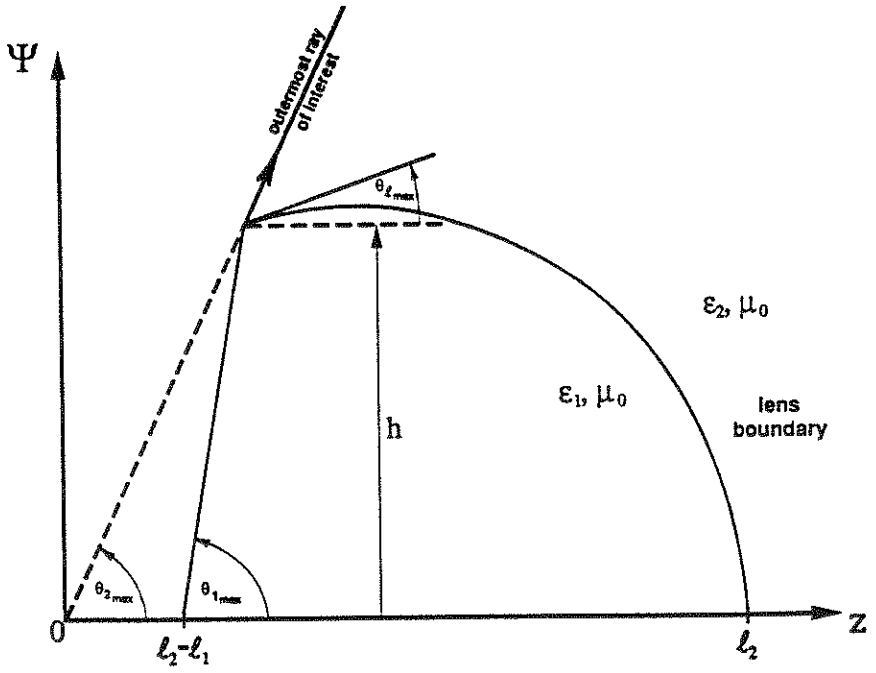

b) Cylindrical coordinate system (Ψ, z) at the feed

Figure 7. Geometry for electromagnetic lens design

b) compute

$$\frac{\ell_1}{h} = \frac{\cos(\theta_{2\max}) + \sqrt{\mathcal{E}_r}\,\sin(\theta_{2\max}) - 1}{(\sqrt{\mathcal{E}_r} - 1)\,\sin(\theta_{2\max})} \simeq 1.4815$$

$$\frac{\ell_2}{h} = \frac{\sqrt{\mathcal{E}_r}\,[\cos(\theta_{2\max}) + \sin(\theta_{2\max})] - 1}{(\sqrt{\mathcal{E}_r} - 1)\,\sin(\theta_{2\max})} \simeq 1.7626$$

$$A = (\ell_2/\ell_1) - 1 = 0.1897$$

$$B = (\ell_2/\ell_1) - \sqrt{\mathcal{E}_r} = -0.3136$$

c) Next, we vary θ_1 from 0 to 90° and compute θ_2 for each θ_1 using [15]

$$\cos(\theta_2) = \frac{AB\,\sin^2(\theta_1) + \left|B\,\cos(\theta_1) - A\sqrt{\mathcal{E}_r}\right| \sqrt{\left[B^2 - 2AB\sqrt{\mathcal{E}_r}\,\cos(\theta_1) + A^2\mathcal{E}_r\right] - A^2\,\sin^2(\theta_1)}}{B^2 - 2AB\,\sqrt{\mathcal{E}_r}\,\cos(\theta_1) + A^2\,\mathcal{E}_r} \tag{12}$$

d) Then, we find the coordinates of the lens boundary using [15],

$$(z/h) = \frac{\tan(\theta_1)\left[\frac{\ell_2}{h} - \frac{\ell_1}{h}\right]}{\tan(\theta_1) - \tan(\theta_2)} = \frac{0.2811\,\tan(\theta_1)}{\tan(\theta_1) - \tan(\theta_2)}$$

$$(\Psi/h) = (z/h)\,\tan(\theta_2) = \frac{0.2811\,\tan(\theta_1)\,\tan(\theta_2)}{\tan(\theta_1) - \tan(\theta_2)} \tag{13}$$

A simple computer routine is written to carry out the steps and the results are indicated in Table 1. This resulted in the fabrication of the lens, as illustrated in the engineering drawing of figure 8. This electromagnetic lens has been incorporated into the design of the pulse generator, which is described in the following section.

4. High-Voltage, Fast Pulse Generator

To maximize the peak far field and its high-frequency content, it was desired to drive the TEM feed lines with a differential ($\pm V_0/2$) high-voltage and a short risetime. We chose an approximate exponential decay in the time-domain voltage pulse, so as to get a smooth radiated spectrum. The e-folding decay time of the voltage pulse was selected to be about 20 ns (large compared to a (10–90)% rise) and sufficiently large to radiate signals down to 50 MHz. This lower limit of frequencies radiated by the reflector IRA arises from the physical size of the reflector (diameter $D = 3.66$ m). Initially, we set a goal of ± 50 kV, ≤ 150 ps (10–90)% risetime, ~ 45 ns (10–90)% fall time, with a prf of 100 Hz. As is seen later, we achieved $> \pm 60$ kV, ~ 100 ps (10–90)% risetime, ~ 45 ns (10–90)% fall time and

$$f_d = (F/D) = 0.33; \quad \theta_{2\max} = 74.29°; \quad \theta_{1\max} = 90°$$

$$\mathcal{E}_r = 2.26$$

θ_1°	θ_2°	z/h	Ψ/h
.00	.00	1.7629	.0000
3.00	2.52	1.7600	.0775
6.00	5.04	1.7522	.1546
9.00	7.56	1.7389	.2309
12.00	10.08	1.7204	.3059
15.00	12.60	1.6969	.3793
18.00	15.12	1.6685	.4507
21.00	17.63	1.6353	.5198
24.00	20.15	1.5976	.5861
27.00	22.66	1.5557	.6494
30.00	25.16	1.5097	.7093
33.00	27.67	1.4601	.7656
36.00	30.17	1.4071	.8180
39.00	32.67	1.3510	.8663
42.00	35.16	1.2922	.9103
45.00	37.65	1.2311	.9499
48.00	40.14	1.1680	.9849
51.00	42.62	1.1033	1.0152
54.00	45.09	1.0374	1.0408
57.00	47.56	.9707	1.0617
60.00	50.03	.9035	1.0778
63.00	52.49	.8362	1.0892
66.00	54.94	.7691	1.0959
69.00	57.38	.7027	1.0981
72.00	59.82	.6373	1.0959
75.00	62.25	.5731	1.0894
78.00	64.68	.5105	1.0788
81.00	67.09	.4498	1.0644
84.00	69.50	.3912	1.0463
87.00	71.90	.3349	1.0247
90.00	74.29	.2812	1.0000

TABLE 1. Geometry of the lens boundary surface

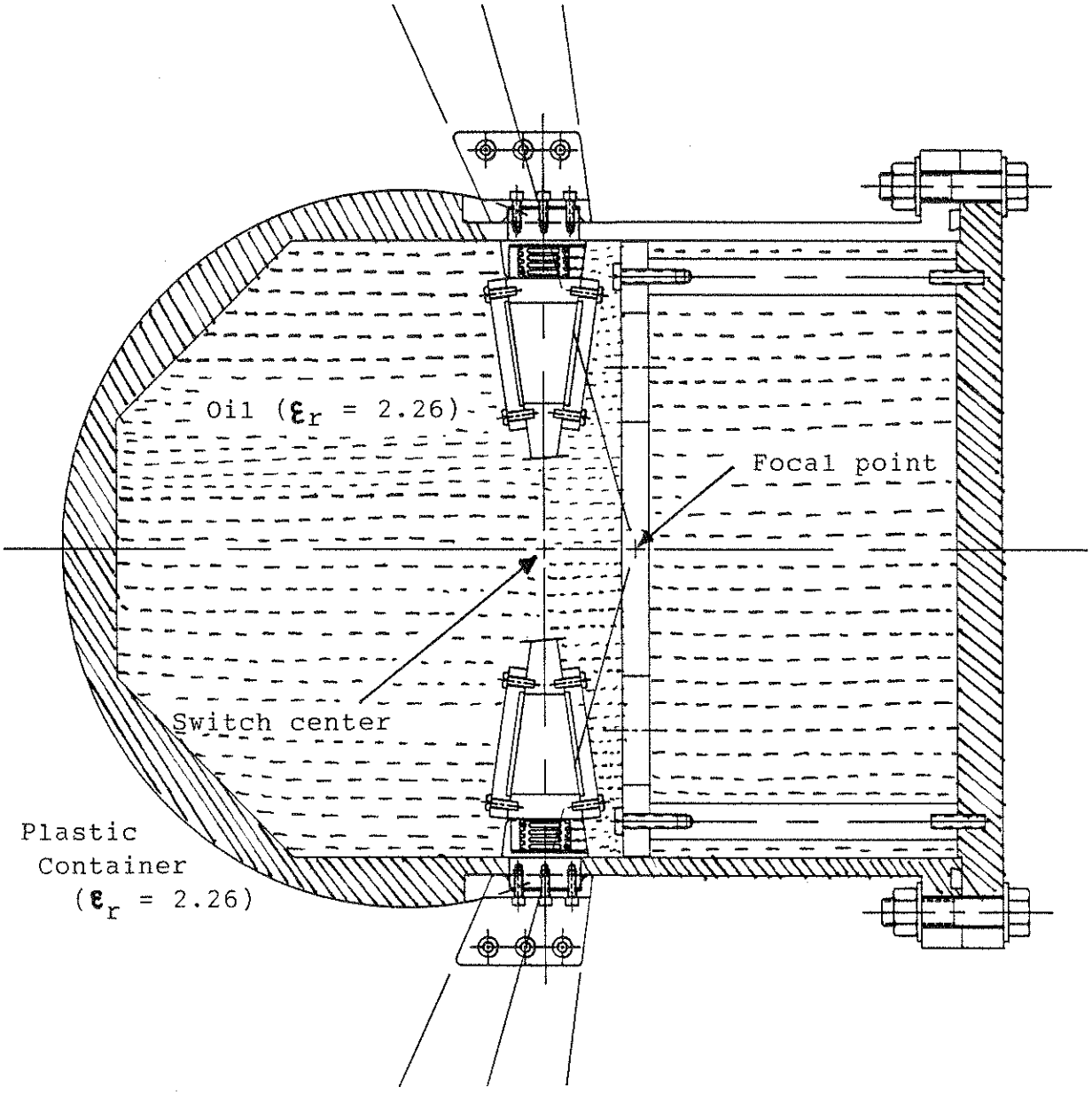

Figure 8. Engineering drawing of the lens geometry

a prf of 200 Hz (maximum). The top and front view of the entire system are shown in figure 9. The major components of the pulser consists of a computer control system, a modulator of primary power with embedded controls/diagnostics, a high-voltage feed assembly and an oil-box assembly containing the output switch and the lens. A simplified schematic of the reflector IRA generator is shown in figure 10. The modulator (dashed rectangle in figure 10) provides the pulsed power and is controlled remotely by fiber optic cables, interfacing with a 486 computer. The computer generates control and trigger signals under control software provided with the system and based on the LabView control language standard. The modulator consists of a small-glass hydrogen thyratron which discharges a 12 nF capacitor into the primary of a step-up pulse transformer. The 12 nF capacitor itself is charged to about 28 kV using a 1 kW cap-charger type of primary power supply. The center-tapped secondary of the pulse transformer differentially charges the ceramic output capacitors in the oil box assembly through the high-voltage feed assembly. Note that the reflector antenna is made to be a part of the charging circuit. The nominal peak charging voltage of ± 60 kV rises in about 220 ns. At this instant, the high pressure ($\sim$ 100 atm) hydrogen switch self-breaks and launches a fast rising wave down the TEM feed lines. The electromagnetic lens made out of the oil medium along with its container ensures an approximate spherical TEM wave centered at the focal point, on the air-medium between the launcher plates. The e-fold decay ($\sim$ 20 ns) of the double exponential pulse is a function of the value of the ceramic capacitors and the TEM impedance (100 pF $\times$ 200 Ω = 20 ns).

The pulse generating system is capable of operation at up to 200 Hz in burst mode. Bursts of 1000 pulses have been achieved, but 500 pulse bursts are typical. Continuous operation at $<$ 10 Hz and single shot modes are both available. The pulser is easy to operate and incorporates numerous safety features. We now turn our attention to expected and measured performance from this prototype reflector IRA.

5. Expected and Measured Performance

Once the design of the reflector IRA is optimized, the quantities of interest are the near and far fields. With regards to the near field, it is well known that a spherical wave illuminating a paraboloidal conducting surface, scatters off as a plane wave focussed at infinity. Near the antenna, one expects an electric field that does not vary with distance (r^0). In the far field, the electric field varies with (r^{-1}). One then is faced with the question of

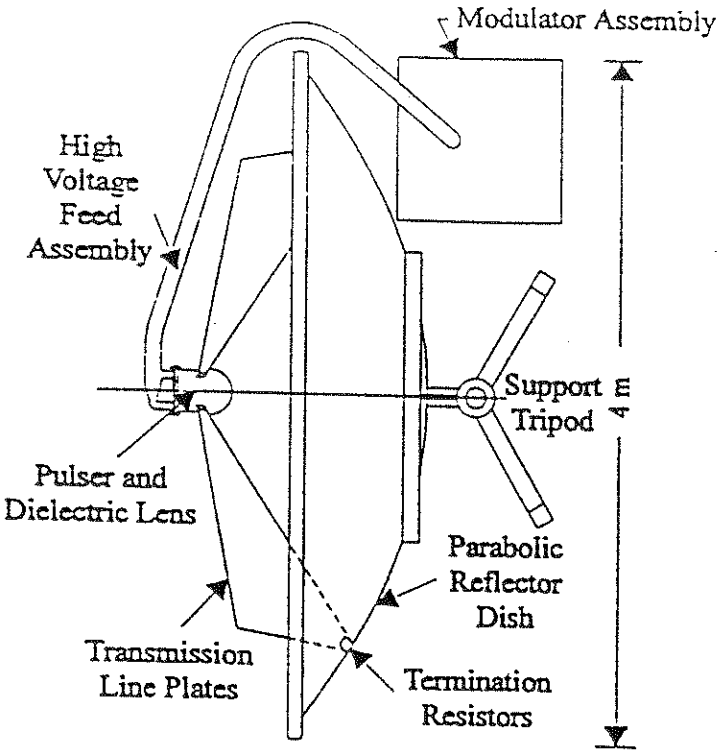

Top View

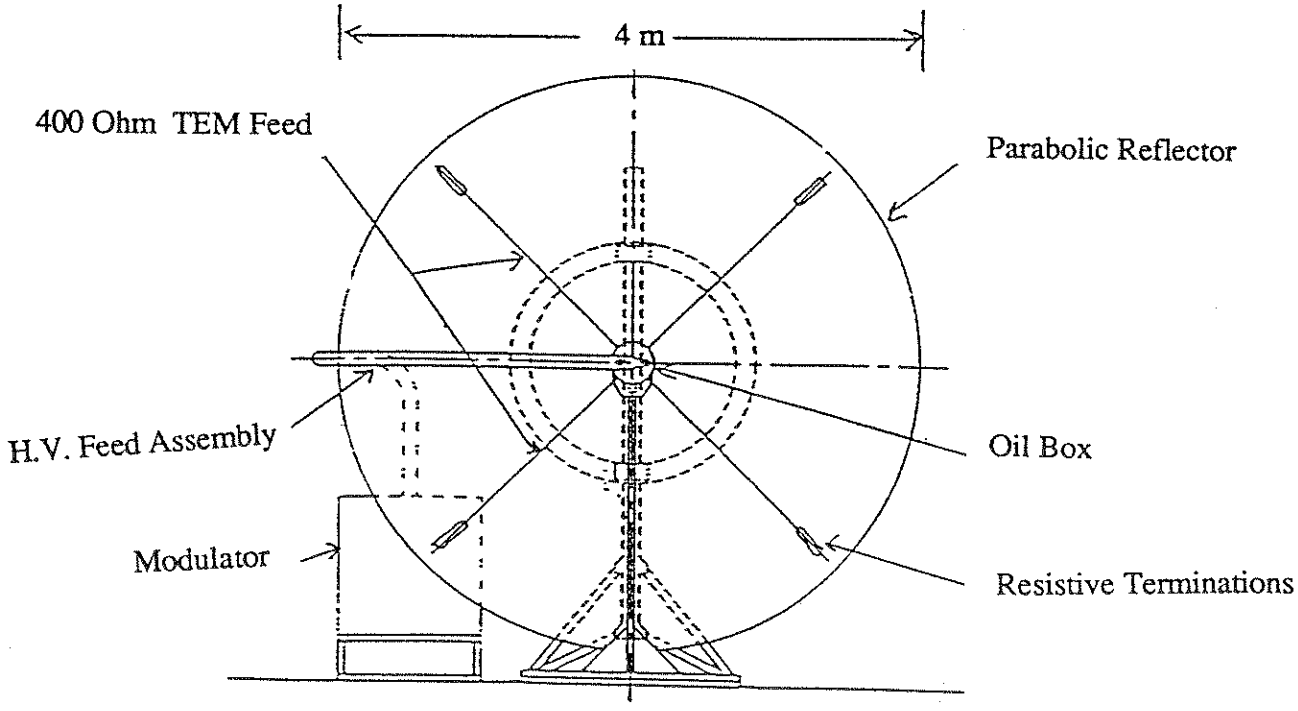

Front View

Figure 9. Top and front views of the prototype reflector IRA system

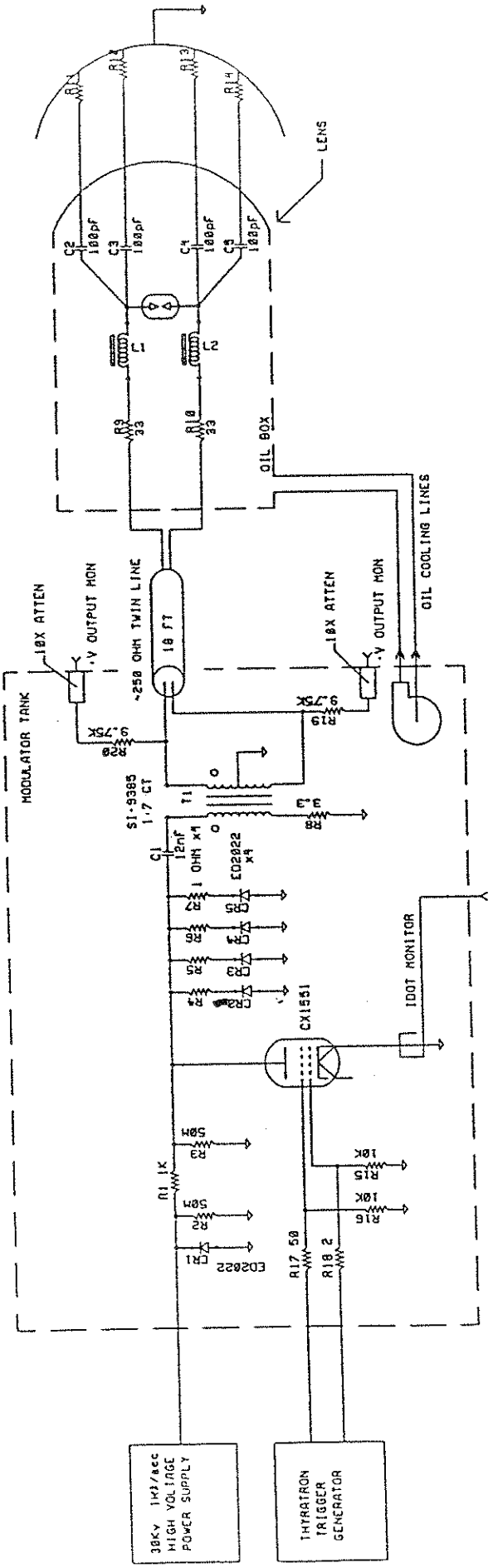

Figure 10. Schematic diagram of the pulse generator in the prototype reflector IRA system

how far away from the antenna, does the far field begin? In the case of CW radiation at a single wavelength λ, the traditional formula is $r \geq 2D^2/\lambda$. This criterion comes from requiring

$$\Delta r \leq \frac{\lambda}{16} \quad \text{or} \quad \frac{\Delta r}{c} \leq \frac{1}{16f} \tag{14}$$

where Δr = differential travel distance to the observer from the center and edge of the antenna. In time-domain applications, we require

$$\frac{\Delta r}{c} < t_{\text{rise}}\ (10-90)\% \tag{15}$$

For the present prototype reflector IRA, when $r = 300$ m $(\Delta r/c) \simeq 19$ ps and is about 20% of the rise time. So, we conclude that for our particular set of antenna dimension ($D = 3.66$ m) and the pulse risetime of ~ 100 ps, the far field begins at a distance of about 300 m.

We may now estimate the near field as follows.

$$\begin{aligned} V_{\text{charge}} &\simeq 120 \text{ kV} \\ V_{\text{switch}} &\simeq 120 \text{ kV} \times 0.8 \simeq 96 \text{ kV} \quad (20\% \text{ losses in the circuit}) \\ V_{\text{plates}} &\simeq V_{\text{switch}} \times \left[\frac{2\sqrt{\varepsilon_r}}{1+\sqrt{\varepsilon_r}}\right] \simeq 115.2 \text{ kV} \end{aligned} \tag{16}$$

It is noted that the voltage on the switch electrodes is enhanced in going from a lower impedance oil medium to the air region. The average electric field in the TEM lines is then given by

$$E_{\text{avg}} \simeq \frac{115.2 \text{ kV}}{3.66 \text{ m}} \times \sqrt{2} \simeq 44.5 \text{ kV/m} \tag{17}$$

The field at the center, or in the horizontal symmetry plane is about 0.77 or 23% less than the average field for a cylindrical two-plate TEM line [16, 17], resulting in an estimated peak electric field of 34.17 kV/m at the center of the parabolic reflector. If one were to measure the near electric field on the optical axis of the reflector, to the right of the feed, the electric field will be somewhat lower than ~ 34 kV/m, owing to the blockage effect caused by the presence of the (switch-lens) oil box. This assembly is in the way of the electromagnetic wave scattered off of the paraboloidal reflector.

In estimating the prepulse amplitude and duration, we can use equation (1) to get

$$\begin{aligned} \text{pre-pulse amplitude} &\simeq -\frac{V_0}{r}\frac{D}{4\pi f_g}\frac{1}{2F}\sqrt{2} \simeq -136 \text{ V/m} \quad \text{at } r = 304 \text{ m} \\ \text{pre-pulse duration} &\simeq \frac{2F}{c} \simeq \frac{2 \times 2.21}{3 \times 10^8} \simeq 8.06 \text{ ns} \end{aligned} \tag{18}$$

In estimating the impulse amplitude, we can use equation (5), to get

$$\text{impulse amplitude} \simeq \frac{V_0}{r}\,\frac{D}{4\pi c f_g}\,\frac{\partial V}{\partial t}\,\sqrt{2}$$

using $D \simeq 3.66$ m, $(\partial V/\partial t) \simeq 10^{15}$ V/s, $c \simeq 3 \times 10^8$ m/s, $f_g = 1.06$, we have [13],

$$\begin{aligned} E_{\text{far}} &\simeq \frac{1550}{r}\ \text{kV/m} \simeq 5\ \text{kV/m (for } r = 305\ \text{m)} \\ \text{or} \quad V_{\text{far}} &= r E_{\text{far}} \simeq 1550\ \text{kV} \end{aligned} \tag{19}$$

Since, we are not sure of and unable to measure $(\partial V/\partial t)$ precisely on the plates, this estimate is at best an approximation. While we know the voltages in the pulser, the precise rate of voltage rise outside the oil box is not known. We believe the estimated V_{far} to be accurate within 15%. If $(\partial V/\partial t)$ has been overestimated by 15%, V_{far} then becomes 1275 kV. The impulse duration at FWHM is roughly the risetime of the input pulse supplied to the reflector IRA.

Having discussed the expected performance of the prototype reflector IRA, we can proceed to report the measured performance. We measured the magnetic field at the center of the reflector using an MGL-7(R) B-dot sensor (risetime 100 ps) and a TDS-820 Tektronix sampling scope (risetime 56 ps). The maximum scope voltage proportional to $\partial B/\partial t$ is seen to be 1.8 V, with a 20 dB attenuation in the signal path (figure 11).

$$\begin{aligned} V_{\text{scope}} &\simeq 1.8\ \text{V (max)} \rightarrow V_{\text{sensor}} \simeq 180\ \text{V (max)} \\ V_{\text{sensor}} &= A(\partial B/\partial t) = (A/c)(\partial E^{(\text{tot})}/\partial t) \\ E^{(\text{inc})} &= \frac{E^{(\text{tot})}}{2} \simeq \frac{V_{\text{sensor}} \times c \times t_{10-90}}{2A} \end{aligned} \tag{20}$$

substituting $V_{\text{sensor}} \simeq 180$ V, $c = 3 \times 10^8$ m/s, $t_{10-90} \simeq 126$ ps and $A \simeq 10^{-4}$ m^2, we have a peak electric incident field of $\sim$ 34 kV/m, which is in excellent agreement with the estimated value of 34.17 kV/m. The measured risetime is 126 ps, but we were instrumentation limited since the field sensor had a risetime of 100 ps and the scope risetime was 56 ps. It is expected that the true risetime is better than 100 ps. In front of the reflector, the peak electric field was measured on axis to be $\sim$ 23 kV/m indicating blockage effect. The blockage effect, while is observable in the near field is not of much significance, when the observer is in the far field, since the far field is the result of spatial

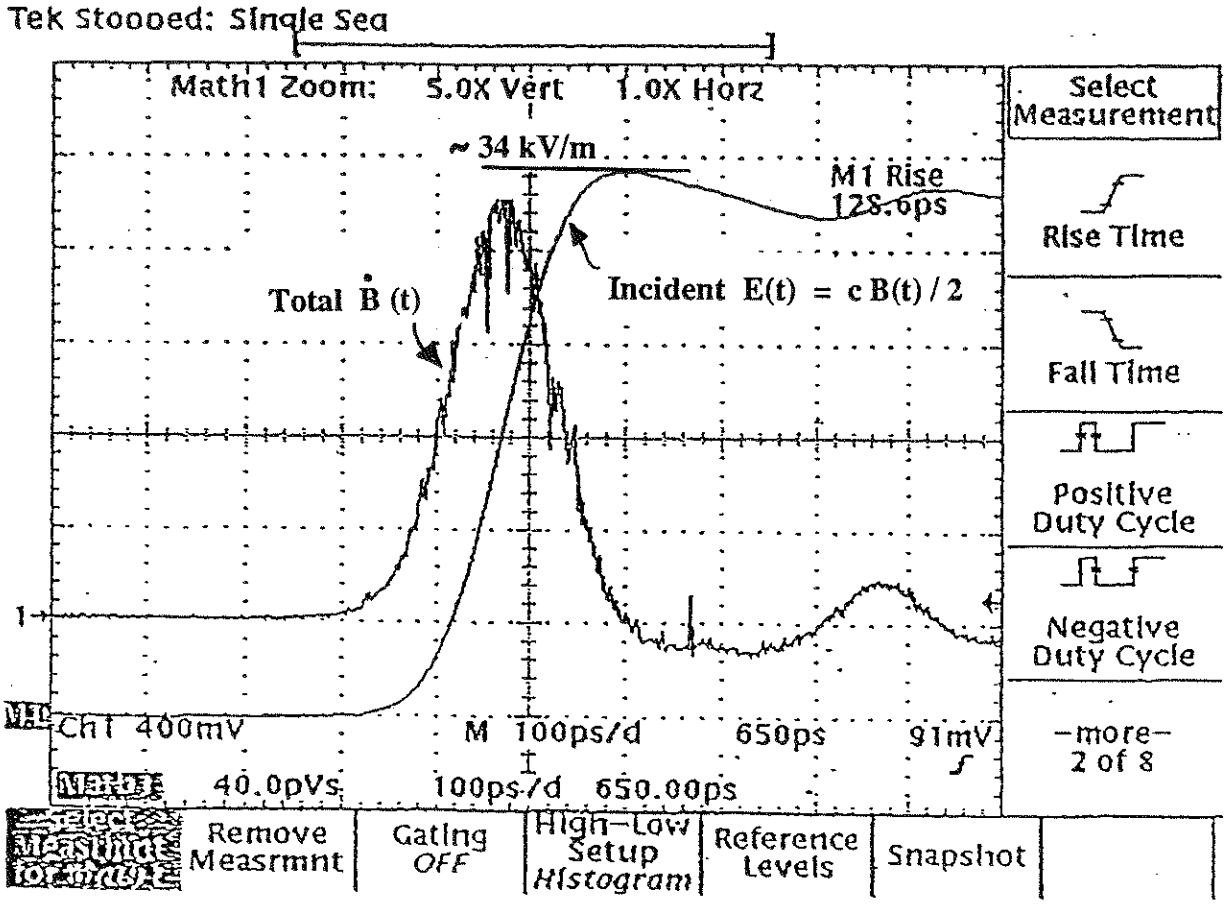

Figure 11. Electric Field at the center of the Reflector from a Measurement of $\dot{B}(t)$ using an MGL -7 (R) Sensor

(± 60 kV, 1400 psi, 200 Hz Operation)

34 kV/m field measurement at 129 ps risetime

Instrumentation limiations:

sensor risetime ~ 100 ps
cable risetime ~ 63 ps
digitizer (TDS 820) risetime ~ 58 ps

V (scope) = 1.8 V
V (sensor) = 180 V = A B(t)
A = 0.0001 sq.m.

integration of the entire aperture field. At a low-voltage excitation, we have also observed the constant electric field amplitude, at distances of 0.5, 1, 2, and 10 m.

An extensive set of far field measurements were performed [18] and a representative waveform at a distance of $r = 305$ m is shown in figure 12 along with the azimuthal variation of the peak electric field in figure 13. A summary of measurements from [18] is listed in Table 2. It is observed that the

$$V_{\text{far}} = r\, E_{\text{far}}(\text{peak}) \simeq 1281 \text{ kV} \tag{21}$$

Measured $(V_{\text{far}}/V_{\text{plates}}) > 10$, is indicative of the highly impulsive behavior of the temporal electric field.

6. Summary

Since it was first proposed in 1989 [1], paraboloidal reflectors fed by TEM transmission lines have received a lot of attention, owing to their main attractive property of extremely wide bandwidth, without the adverse effects of dispersion. All of the frequencies contained in the supplied voltage pulse travel at the same speed on the antenna and arrive at the same time at a distant observer. The bandwidth associated with time-domain antennas is to be distinguished from the approximately 10 to 1 bandwidth of the so called frequency independent antennas such as the log-periodic antenna, which is highly dispersive since the phase center of the antenna is not fixed. Different CW frequencies applied to a log-periodic antenna get radiated from different portions of the antenna, which makes it dispersive, if all of the frequencies are applied at the same time as in a pulsed application. Reflector IRAs overcome this problem and even have equivalent electric and magnetic dipole moments characterizing the low-frequence performance. Even the di-polar radiation at low frequencies is along the optical axis of the reflector. Based on past analytical efforts, an optimal reflector IRA has been designed, fabricated and tested. It produces an impulse-like electric field waveform with a peak amplitude of ~ 4.2 kV/m and a FWHM $\simeq 130$ ps at a distance of 305 m from the antenna. This results in a $V_{\text{far}} = rE_{\text{far}}$ of ~ 1281 kV. Extremely wide bandwidth offered by this reflector IRA is very useful in hostile target identification applications. It this antenna were to be aimed straight up in the sky, it could produce a peak field of 20 V/m at a distance $r = 60$ km, on the bottom layers of the ionosphere. On the ground, the average power at a prf of 200 Hz is of the order of 200 W.

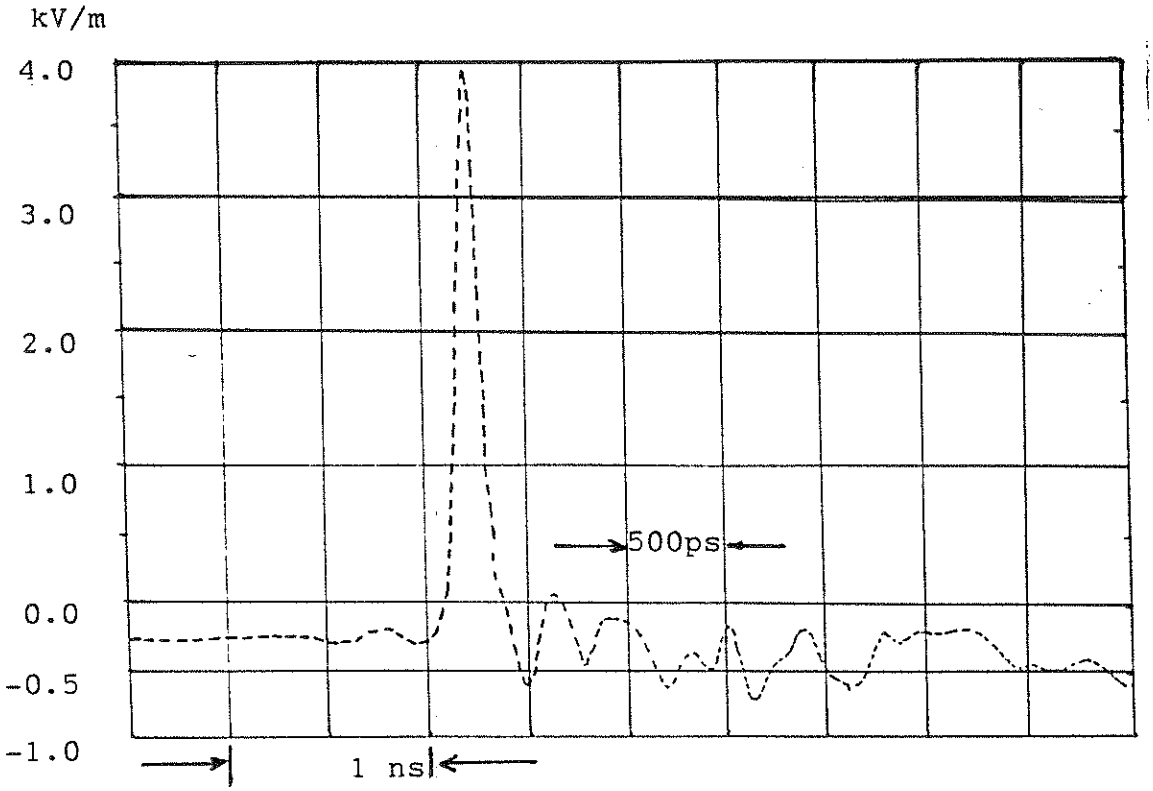

Figure 12. Far electric field at a distance of r = 305 m from the prototype IRA

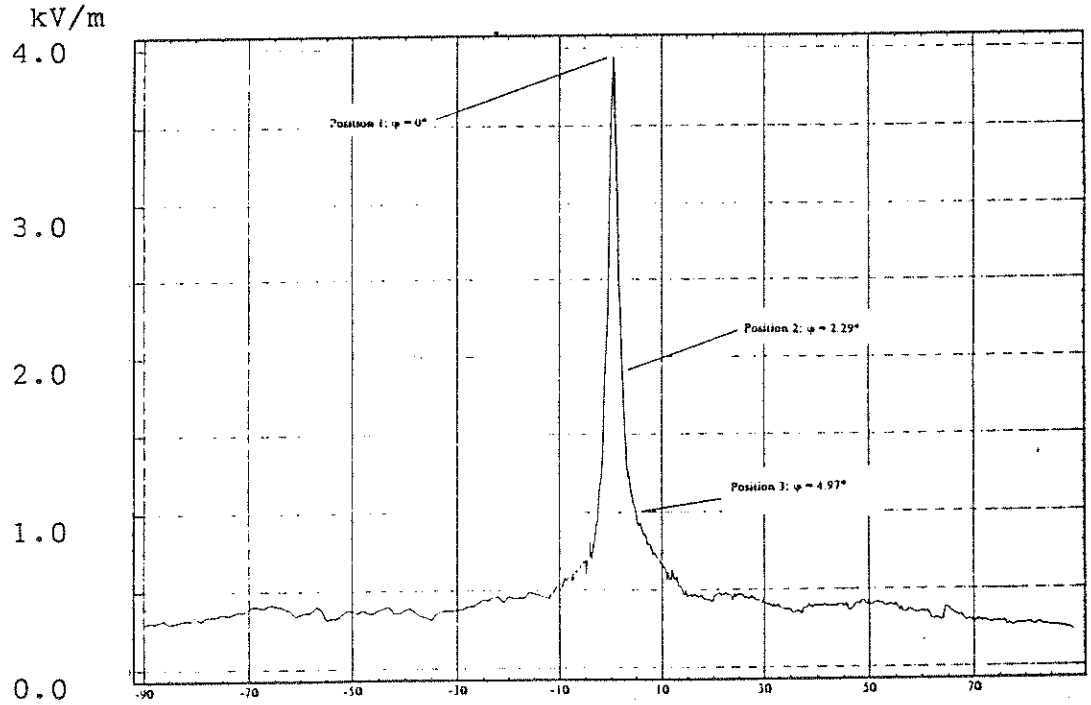

Figure 13. Azimuthal varaiation of the peak of the impulse-like waveform

Physical quantity	Numerical value
Peak electric field on boresight at $r = 305$ m	4.2 kV/m
Boresight electric field (10–90)% risetime, $r = 305$ m	99 ps
Boresight impulse duration (FWHM), $r = 305$ m	130 ps
Boresight electric field spectrum, $r = 305$ m	< 12 db variation over 50 MHz–4 GHz
Main beam scan	
FWHM θ - beam width	$-1.77°$, $+1.45°$
FWHM ϕ - beam width	$-0.98°$, $+2.31°$
Azimuthal, or H-plane pattern	
FWHM ϕ - beam width	3.18°
-3 dB peak power beam width	1.80°
Incident electric field at the center of the dish	~ 34 kV/m
(10–90)% risetime	126 ps*
$V_{\text{far}} = rE_{\text{far}}$	~ 1281 kV

*(instrumentation limited sensor ~ 100 ps, scope ~ 56 ps)

TABLE 2. Summary of the reflector IRA measurements [18]

With increased repetition rate, and enhanced average power into kW regime, electronic warfare applications become possible over a wide band (10's of MHz to several GHz) of frequencies, and over distances of several km. The experimental results reported here testify to the usefulness and desirability of such antennas, which can be built to different sizes and frequency ranges tailored to specific applications.

Acknowledgment

The authors are thankful to Dr. D. Voss, Dr. C. Courtney of Voss Scientific in Albuquerque and Mr. P. Pelletier of Maxwell Laboratories in Albuquerque for their asistance in carrying out an extensive set of far field measurements at the HERTF facility of Phillips Laboratory, Kirtland AFB, NM. A small representative data set is included here and interested readers are encouraged to contact the authors for additional information and/or copies of some of the cited references.

References

1. C. E. Baum, "Radiation of Impulse-Like Transient Fields," *Sensor and Simulation Note* 321, 25 November 1989.
2. C. E. Baum, "Configurations of TEM Feed for an IRA," *Sensor and Simulation Note* 327, 27 April 1991.
3. C. E. Baum, "Aperture Efficiencies for IRAs," *Sensor and Simulation Note* 328, 24 June 1991.
4. E. G. Farr, "Analysis of the Impulse Radiating Antenna," *Sensor and Simulation Note* 329, 24 July 1991.
5. E. G. Farr and C. E. Baum, "Prepulse Associated with the TEM Feed of an Impulse Radiating Antenna," *Sensor and Simulation Note* 337, March 1992.
6. C. E. Baum and E. G. Farr, "Impulse Radiating Antennas," in *Ultra-Wideband, Short-Pulse Electromagnetics.* edited by H. L. Bertoni et al., pp. 139–147, Plenum Press, NY, 1993.
7. D. V. Giri and S. Y. Chu, "On the Low-Frequency Electric Dipole Moment of Impulse Radiating Antennas (IRAs)," *Sensor and Simulation Note* 346, 5 October 1992.
8. E. G. Farr, "Optimizing the Feed Impedance of Impulse Radiating Antennas Part I: Reflector IRAs," *Sensor and Simulation Note* 354, January 1993.
9. D. V. Giri and C. E. Baum, "Reflector IRA Design and Boresight Temporal Wave-

forms," *Sensor and Simulation Note* 365, 2 February 1994.

10. D. V. Giri and H. Lackner, "Fabricational Details of Prototype IRAs," *Prototype IRA Memo* 1, 1 May 1994.
11. D. V. Giri and H. Lackner, "Preliminary Evaluation of the Terminating Impedance in the Conical-Line Feed of IRAs," *Prototype IRA Memo* 2, 15 May 1994.
12. D. V. Giri, "Design Considerations of a Uniform Dielectric Lens for Launching a Spherical TEM Wave onto the Prototype IRA," *Prototype IRA Memo* 3, 15 May 1994.
13. D. V. Giri and H. Lackner, "Estimates of Peak Values of Near and Far Fields of Prototype IRAs," *Prototype IRA Memo* 4, 15 May 1994.
14. J. B. Keller and A. Blank, "Diffraction and Reflection of Pulses by Wedges and Corners," *Communications on Pure and Applied Mathematics*, Volume 4, 1951, pp. 75–94.
15. C. E. Baum, J. J. Sadler, and A. P. Stone, "A Uniform Dielectric for Launching a Spherical Wave into a Paraboloidal Reflector," *Sensor and Simulation Note* 360, 22 July 1993.
16. C. E. Baum, D. V. Giri, and R. D. Gonzalez, "Electromagnetic Field Distribution of the TEM Mode in a Symmetrical Two-Parallel-Plate Transmission Line," *Sensor and Simulation Note* 219, 1 April 1976.
17. F. C. Yang and L. Marin, "Field Distributions on a Two-Conical-Plate and a Curved Cylindrical-Plate Transmission Line," *Sensor and Simulation Note* 229, September 1977.
18. C. C. Courtney, Voss Scientific, Private communication, April 1995.